ENVIRONMENTAL RESEARCH
LETTERS

LETTER • OPEN ACCESS

The 11 year solar cycle UV irradiance effect and its dependency on the Pacific Decadal Oscillation

To cite this article: Sigmund Guttu *et al* 2021 *Environ. Res. Lett.* **16** 064030

ENVIRONMENTAL RESEARCH
LETTERS

LETTER

The 11 year solar cycle UV irradiance effect and its dependency on the Pacific Decadal Oscillation

Sigmund Guttu[1], **Yvan Orsolini**[2,3], **Frode Stordal**[1], **Odd Helge Otterå**[4] and **Nour-Eddine Omrani**[5]

[1] University of Oslo, Oslo, Norway
[2] Norwegian Institute for Air Research, Kjeller, Norway
[3] Department of Physics, NTNU, Trondheim, Norway
[4] NORCE Norwegian Research Centre AS, Bjerknes Centre for Climate Research, Bergen, Norway
[5] University of Bergen, Bergen, Norway

E-mail: sigmund.guttu@geo.uio.no

OPEN ACCESS

RECEIVED
2 February 2021

REVISED
9 April 2021

ACCEPTED FOR PUBLICATION
6 May 2021

PUBLISHED
24 May 2021

Keywords: 11 year solar cycle, polar vortex, Pacific Decadal Oscillation, Aleutian Low

Supplementary material for this article is available online

Abstract

The stratospheric, tropospheric and surface impacts from the 11 year ultraviolet solar spectral irradiance (SSI) variability have been extensively studied using climate models and observations. Here, we demonstrate using idealized model simulations that the Pacific Decadal Oscillation (PDO), which has been shown to impact the tropospheric and stratospheric circulation from sub-decadal to multi-decadal timescales, strongly modulates the solar-induced atmospheric response. To this end, we use a high-top version of the coupled ocean–atmosphere Norwegian Climate Prediction Model forced by the SSI dataset recommended for Coupled Model Intercomparison Project 6. We perform a 24-member ensemble experiment over the solar cycle 23 in an idealized framework. To assess the PDO modulation of the solar signal, we divide the model data into the two PDO phases, PDO+ and PDO−, for each solar (maximum or minimum) phase. By compositing and combining the four categories, we hence determine the component of the solar signal that is independent of the PDO and the modulation of the solar signal by the PDO, along with the solar signal in each PDO phase. Reciprocally, we determine the PDO effect in each solar phase. Our results show that the intensification of the polar vortex under solar maximum is much stronger in the PDO− phase. This signal is transferred into the troposphere, where we find a correspondingly stronger polar jet and weaker Aleutian Low. We further show that the amplification of the solar signal by the PDO− phase is driven by anomalous meridional advection of solar-induced temperature anomalies over northern North America and the North Pacific, which contributes to a decreased meridional eddy heat flux and hence to a decreased vertical planetary wave flux into the stratosphere.

1. Introduction

The stratospheric, tropospheric and surface impacts from the 11 year ultraviolet (UV) solar spectral irradiance (SSI) variability have been extensively studied during recent years using climate models and observations (see Gray *et al* (2010) or Matthes *et al* (2017) for reviews; Mitchell *et al* 2015, Misios *et al* 2015). Under more intense heating from the UV component of the SSI during solar maximum conditions, an increase in the upper-stratospheric meridional temperature gradient between low and high latitudes develops, associated to a strengthened wintertime stratospheric polar vortex. A top-down mechanism involving wave-mean flow interaction (Kodera and Kuroda 2002) then allows for the downward seasonal migration of the zonal-mean zonal wind anomaly throughout the stratosphere, with subsequent impacts in the troposphere and at the surface, both globally and regionally. The SSI-induced top-down stratospheric influence manifests itself prominently in the North Atlantic region, where both observational and model studies (Gray *et al* 2013, Scaife *et al* 2013, Andrews *et al* 2015, Ma *et al* 2018) have suggested a tendency for a more positive phase of the North Atlantic Oscillation, albeit with a lag of a few

years with respect to the solar maximum, explained in terms of ocean–atmosphere coupling.

Surface signals associated to the 11 year solar cycle variability in SSI and in total solar irradiance (TSI) have also been identified over the Pacific sector. In observations, as well as in models, a surface pressure signal over the North Pacific during solar maximum has been found to contribute to a weakening of the Aleutian Low, the dominant winter-time low pressure center over the North Pacific (Meehl *et al* 2008, Roy and Haigh 2010, Ineson *et al* 2011, Gray *et al* 2013, Hood *et al* 2013, Roy 2014). Furthermore, based on the examination of the extended sea surface temperature (SST) records from the mid-19th century to recent years, several studies determined that solar maximum conditions predominantly corresponded to SST anomalies characteristic of the Pacific Decadal Oscillation (PDO) negative phase (van Loon *et al* 2007, Kren *et al* 2016). The SSTs over the mid-latitudes of the North Pacific Ocean play an important role in the climate system, since this region is situated at the confluence of warm and cold currents near 40° N, a hotspot of climate variability (Yukimoto *et al* 2017). Further south, over the tropical Pacific, the impact of the TSI variability drives a so-called bottom-up mechanism, by which direct solar heating of the sea surface in cloud free areas and subsequent ocean–atmosphere interactions involving water vapor, convection and clouds, modify the Hadley and Walker circulations and amplify the solar signal (Meehl *et al* 2009, Misios *et al* 2015). By analyzing models with and without the stratospheric SSI forcing and either prescribed SST or interactive ocean–atmosphere coupling, Meehl *et al* (2009) provided further evidence that the TSI and SSI act in concert to induce the solar signatures in the tropical Pacific, a conclusion also confirmed by Rind *et al* (2008). The changes in precipitation over the tropical and subtropical Pacific then induce propagation of quasi-stationary wavetrains northeastwards into the extratropics (Meehl *et al* 2008).

The PDO is a dominant, coupled mode of climate variability over the North Pacific Ocean varying on interannual, sub-decadal and multi-decadal time scales (Mantua *et al* 1997; see Newman *et al* 2016 for a review). Traditionally, it is defined as the first principal component of the Pacific SST north of 20° N. In its negative phase it takes the form of a horseshoe pattern, with warm anomalies in the western and central North Pacific and opposite anomalies in the Gulf of Alaska, along the west coast of North America and over the eastern and central tropical Pacific. The PDO is an internal climate mode that is particularly important for the winter-time weather and climate in the Pacific region, owing to key teleconnections to North America (such as the Pacific-North American pattern) and further east to Europe and Eurasia. It is hence associated to global climate impacts (Newman *et al* 2016). The PDO likely results from a combination of different processes across a wide range of latitudes, encompassing the El Niño–Southern Oscillation (ENSO) in the tropical Pacific and atmospheric forcing through wind stress over the extratropical North Pacific (Newman *et al* 2016, Wills *et al* 2018). The sub-decadal PDO variability is often considered to be a manifestation of ENSO. A recent study aimed at disentangling the ENSO-related and the extratropical North Pacific variability embedded in the traditional PDO index (Wills *et al* 2018) rather suggests that the latter, which is driven by the atmospheric forcing, has an even more pronounced decadal variability than the PDO signal captured by the traditional index, which encompasses both sources of variability.

The modulation of the intensity of the Aleutian Low by the PDO exerts a key influence on the polar stratospheric circulation, a fact supported by several model and observational studies (Jadin *et al* 2010, Hurwitz *et al* 2012, Woo *et al* 2015, Kren *et al* 2016, Hu and Guan 2018, Li *et al* 2018). In the PDO negative phase (PDO−), the polar vortex tends to be stronger than normal, while it tends to be weaker in the PDO positive phase (PDO+). The explanation relies on the variability of upward-propagating planetary waves (Woo *et al* 2015, Kren *et al* 2016, Hu and Guan 2018, Hu *et al* 2018): when the Aleutian Low weakens in PDO−, there is a tendency for lessened planetary wave activity, which leads to a stronger polar vortex. The far East/North-western Pacific region is the center of the largest climatological wave activity flux into the stratosphere and has thereby the potential to exert a strong forcing onto the middle atmosphere. Supporting the key influence of the North Pacific mid and high-latitude circulation upon the polar stratosphere, the Western Pacific climate pattern, which is characterized by a meridionally oriented dipole of height anomalies, was shown to have the strongest influence on polar stratospheric temperatures among the dominant mid-tropospheric patterns of climate variability, surpassing ENSO (Orsolini *et al* 2009, Nishii *et al* 2010). While the PDO influence on the middle atmosphere was investigated in a multi-centennial control simulation of Whole Atmosphere Community Climate Model (WACCM) coupled to another ocean model by Kren *et al* (2016), the PDO modulation of the solar signal was not addressed. In summary, the PDO may precondition the tropospheric and the stratospheric circulation (e.g. a PDO− phase leading to a stronger polar vortex), which could modulate the response to external climate forcings (e.g. Dong *et al* (2014)). A relevant question is to what extent the dynamical impacts from the SSI variations associated to the 11 year solar cycle are modulated by the PDO phase.

Hence, we aim to examine the extent to which the top-down SSI effects on the stratosphere and on the tropospheric climate depend on the PDO phase. This is carried out in an idealized framework

where we conduct an ensemble of decadal simulations for present-day climate conditions covering a single 11 year solar cycle (specifically solar cycle 23 (SC-23)), with its associated SSI variability. We keep the forcing from volcanic activity constant, and do not prescribe the quasi-biennial oscillation (QBO). The lack of a prescribed QBO means that the zonal-mean zonal winds in the tropical stratosphere remain predominantly westward. This idealized approach is hence more focused on identifying clear pathways, that might be masked or aliased in a comprehensive, transient multi-decadal coupled run as obtained from the Coupled Model Intercomparison Project (CMIP) 6 for example. To that end, we use a version of the Norwegian Climate Prediction Model (NorCPM), where a high-top chemistry-climate model (WACCM) is coupled to an ocean model (Miami Isopycnic Coordinate Model (MICOM)) (Li *et al* 2019). To assess the PDO modulation of the solar signal, we divide the model data into the two PDO phases, PDO+ and PDO−, for each solar (maximum or minimum) phase. By compositing and combining the four categories, we hence determine the component of the solar response that is independent of the PDO, the solar response in each PDO phase and its modulation by the PDO. Reciprocally, we can also determine any PDO response to the solar forcing. Such a quasi-linear approach was adopted by Screen and Francis (2016), who studied the interplay between the impacts of Arctic sea ice loss and the PDO phase. We focus on the early winter period when the internal variability of the polar stratosphere is weaker than in late winter (e.g. Ayarzaguëna *et al* (2013)).

2. Methods

In this study, we use the high-top variant of NorCPM described in Li *et al* (2019). NorCPM is a prediction system that combines the Norwegian Earth System Model (Bentsen *et al* 2013) with a data assimilation-based initialization. The high-top variant of NorCPM comprises the Community Earth System Model version 1.0.3 including the fully interactive chemistry and dynamical model WACCM4 coupled to the ocean model MICOM. WACCM extends up to 5×10^{-6} hPa (∼140 km) and the vertical domain incorporates 66 layers of variable vertical resolution. The horizontal atmospheric resolution in this study is 1° latitude by 2° longitude. Detailed descriptions of WACCM can be found in previous studies on solar effects (e.g. Marsh *et al* (2007)) and in the WACCM4 documentation (Neale *et al* 2012). The ocean component is an updated version of MICOM (Bleck *et al* 1992) with a horizontal resolution of 1° by 1° and involves 53 vertical layers.

As a time-varying SSI forcing, we follow the recommendation for CMIP6 (Matthes *et al* 2017). The SSI time series is an average of two solar irradiance models, i.e. the empirical NRLSSI2 (Coddington *et al* 2016) and the semi-empirical SATIRE-T/S (Yeo *et al* 2015). Compared to the CMIP5 data based on Wang *et al* (2005), the 200–400 nm wavelength range irradiance contributes to a larger portion of the TSI solar-cycle variability. The modeled period mostly covers SC 23 (August 1996–November 2008), but since the model experiment is from a set of experiments considering Medium-Energy Electron forcing from 1998, the initial period of low solar activity from August 1996 to August 1998 is replaced by a near-identical period of SC 24 (November 2008–August 2010).

To ensure that the simulations start from an equilibrated state, we ran a spin-up of NorCPM with a constant solar forcing, covering 86 years in total. Initialized in year 50 of this spin-up run (which we will refer to as the background run), a 12 year ensemble simulation of 24 members was carried out. Each ensemble member is generated by applying a small initial temperature perturbation of the order of 10^{-14}, based on the procedure in Kay *et al* (2015).

The November–December (ND) PDO indices are calculated based on a regional (20–60° N, 140° E–120° W) empirical orthogonal function (EOF) analysis of the SST from the last 50 years of the background run. The SST anomalies of each ensemble member, i.e. the deviation from their respective climatology, are then projected onto the first EOF from the background run to obtain an ensemble of PDO time series (see figure S1 (available online at stacks.iop.org/ERL/16/064030/mmedia)). The PDO positive (negative) phase corresponds to all positive (negative) values of the PDO index. All 24 members of the ensemble decadal simulation start from a PDO− phase that prevailed at the initialization time.

In figure 1(a), we show the monthly mean time series of the UV SSI forcing throughout the solar cycle, with the four years that we consider as solar maximum (hereafter Smax) and solar minimum (hereafter Smin) years indicated. Then, in figure 1(b), we show the ND PDO indices during those four Smax and Smin years across the different members. Hereafter, we sort these data into four groups of comparable size according to the solar and the PDO phases that prevailed in these early winter periods, denoted SmaxPDO+, SmaxPDO−, SminPDO+ and SminPDO−. For example, the group SmaxPDO+ corresponds to the 52 early winter cases when a PDO+ occurred at the same time as Smax. Figure 1(c) shows the probability density distribution of the PDO index in each solar phase. The similarity of the two distributions already suggests that there is no robust solar cycle influence upon the PDO index, and we will return to that point later.

We first estimate the solar response independent of (i.e. irrespective of) the PDO phase, denoted $(\text{Smax} - \text{Smin})_{\text{allmembers}}$. We next estimate the

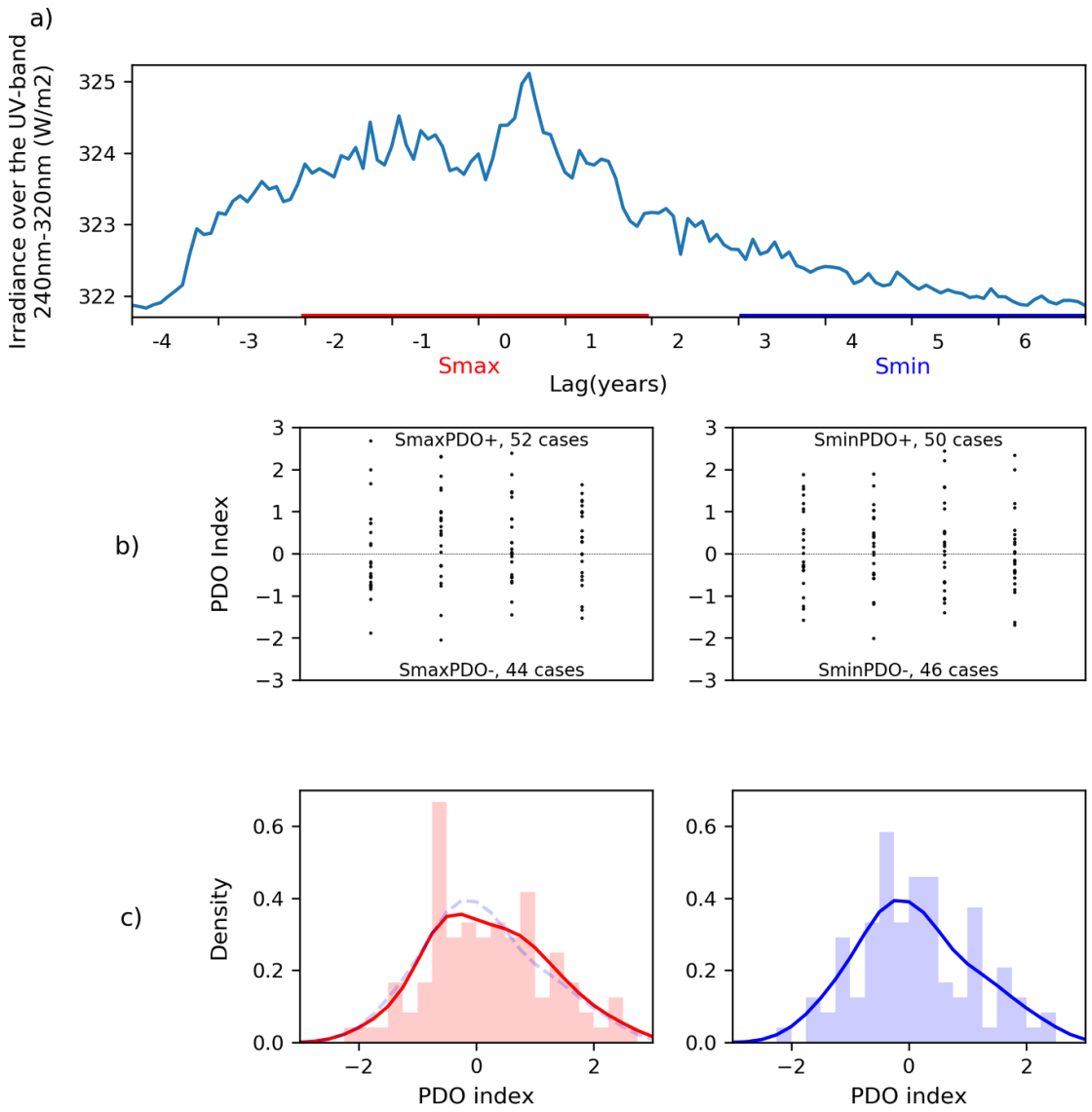

Figure 1. The monthly mean solar irradiance forcing averaged over the 240–320 nm spectral wavelength band over the solar cycle is shown in (a). The periods used as Smax (Smin) are indicated in red (blue). (b) The ND PDO index of all cases within the ensemble (dots) for each year in Smax and Smin. The dashed line indicates PDO = 0 which was used as the criterion for dividing both Smax and Smin into PDO+ and PDO−. The four groups are indicated, also with their respective number of cases. In (c), we show the PDO density histogram and corresponding Gaussian distribution fit for the Smax and Smin groups shown in (b). The dashed blue line in Smax is the same as the blue solid line in Smin, repeated for clarity.

solar response in PDO+ as the mean difference between the SmaxPDO+ and SminPDO+ groups, denoted $(\text{Smax} - \text{Smin})_{\text{PDO+}}$, and in PDO− as the mean difference between the SmaxPDO− and SminPDO− groups, denoted $(\text{Smax} - \text{Smin})_{\text{PDO−}}$. To estimate the modulation of the solar response by the PDO, i.e. the dependence of the solar response upon the phase of the PDO, we subtract the aforementioned differences to obtain $(\text{Smax} - \text{Smin})_{\text{PDO−}} - (\text{Smax} - \text{Smin})_{\text{PDO+}}$. Note that, in this paper, the PDO difference is always taken as PDO− minus PDO+, as we want to emphasize the negative PDO effects. Reciprocally, we estimate the PDO response independent of the solar phase, denoted $(\text{PDO−} - \text{PDO+})_{\text{allmembers}}$, and the PDO response during each solar phase as the mean differences SmaxPDO− − SmaxPDO+, denoted $(\text{PDO−} - \text{PDO+})_{\text{Smax,}}$ and SminPDO− − SminPDO+, denoted $(\text{PDO−} - \text{PDO+})_{\text{Smin}}$. The solar modulation of the PDO response, $(\text{PDO−} - \text{PDO+})_{\text{Smax}} - (\text{PDO−} - \text{PDO+})_{\text{Smin,}}$ can be shown to be equal to the aforementioned PDO modulation of the solar response by re-arranging the linear combinations. Table 1 summarizes these various combinations.

We also use the near-real-time UK Hadley Centre Sea Level Pressure (HadSLP2r) data set (Ansell *et al* 2006) over the period 1854–2017. To group the observational data according to the solar and the PDO phases, we use corresponding time series of the PDO index and UV SSI. The SmaxPDO+, SmaxPDO−, SminPDO+ and SminPDO− groups contain 29, 31, 32 and 28 cases, respectively (see figure S1 for comparison with the model data). In figure S2, we show

Table 1. Solar and PDO responses according to solar and PDO phases.

Responses		Description
Solar responses	Groups used	
$(\text{Smax} - \text{Smin})_{\text{allmembers}}$	SmaxPDO−,SminPDO−, SmaxPDO+, SminPDO+	The total solar response independent of the PDO
$(\text{Smax} - \text{Smin})_{\text{PDO}-}$	SmaxPDO−, SminPDO−	The solar response in PDO−
$(\text{Smax} - \text{Smin})_{\text{PDO}+}$	SmaxPDO+, SminPDO+	The solar response in PDO+
$(\text{Smax} - \text{Smin})_{\text{PDO}-} - (\text{Smax} - \text{Smin})_{\text{PDO}+}$	SmaxPDO−, SminPDO−, SmaxPDO+, SminPDO+	The solar response modulated by the PDO effect
PDO responses	Groups	
$(\text{PDO}- - \text{PDO}+)_{\text{allmembers}}$	All members, all years	The total PDO effect independent of solar phase
$(\text{PDO}- - \text{PDO}+)_{\text{Smax}}$	SmaxPDO−, SmaxPDO+	The PDO response in Smax
$(\text{PDO}- - \text{PDO}+)_{\text{Smin}}$	SminPDO−, SminPDO+	The PDO response in Smin
$(\text{PDO}- - \text{PDO}+)_{\text{Smax}} - (\text{PDO}- - \text{PDO}+)_{\text{Smin}}$	SmaxPDO−, SminPDO−, SmaxPDO+, SminPDO+	The PDO response modulated by the solar effect

the observational PDO index derived using the same EOF approach on the NOAA Extended Reconstructed SST V5 (Huang *et al* 2017), and the UV SSI, again retrieved from the historical CMIP6 data.

In the following section, we show ND averages of the terms defined in table 1. We have calculated the statistical significance on a 95% confidence level by performing a permutation or Monte-Carlo test. The 10^4 randomized samples are taken among the Smax and Smin years in the 24-member ensemble. The solar-induced anomaly (ensemble mean) is then compared with this distribution to estimate a confidence level. In the figures, statistically significant regions at the 95% (90%) confidence level are indicated by large (small) colored dots.

3. Results

First, we verify that our simulations capture the well-known PDO impacts on the troposphere and the stratosphere. To that end, we show in figure 2 the early winter mean (ND) PDO and its atmospheric impacts in terms of SLP, zonal winds at 200 hPa and zonal-mean zonal winds from surface up to the mesopause region (10^{-2} hPa), independently of solar forcing, i.e. $(\text{PDO}- - \text{PDO}+)_{\text{allmembers}}$ (see table 1). Figure 2(a) shows the typical PDO− pattern in SST, with the mid-latitude central North Pacific Ocean characterized by positive anomalies and the remaining aforementioned horseshoe pattern of cold anomalies. Figure 2(b) shows the characteristic anticyclonic anomaly in the Aleutian Low region, i.e. corresponding to a weakening of the latter, with anomalous westward winds at its southern edge weakening the subtropical jet stream across the Pacific and anomalous eastward winds at its northern edge strengthening the upper-tropospheric polar jet (figure 2(c)). These changes are not limited to the upper tropospheric jets and are clearly seen as a meridional dipole of zonal-mean zonal wind anomalies throughout the troposphere, with a weakening centered around 35° N and an increase at high latitudes (figure 2(d)). The latter contributes to a weak negative SLP anomaly over the Arctic, as seen in figure 2(b) (see also in Kren *et al* (2016)). As the Aleutian Low weakening reduces the planetary wave forcing into the stratosphere, the polar vortex intensifies throughout the stratosphere (figure 2(d)).

Previous studies have shown that the UV SSI increase in Smax leads to a strengthened winter stratospheric polar vortex (see section 1). Our simulated zonal-mean zonal wind differences for the solar response independent of the PDO phase, $(\text{Smax} - \text{Smin})_{\text{allmembers}}$, are consistent with these findings (figure 3(a)). However, the magnitudes of the anomalies are also strongly dependent of the PDO phase, with a more pronounced strengthening of the stratospheric jet during PDO− ($(\text{Smax} - \text{Smin})_{\text{PDO}-}$) compared to PDO+ ($(\text{Smax} - \text{Smin})_{\text{PDO}-}$) (figures 3(b) and (c)). The zonal winds anomalies independent of the PDO phase are relatively weak, up to 5 m s^{-1} in the core of the polar night jet near the stratopause, while in PDO−, the zonal wind changes are stronger (over 8 m s^{-1}) and significant over a broad region that extends from the upper troposphere to the lower mesosphere, and over a wide latitudinal band (figure 3(a)). In PDO+, the corresponding anomalies are not significant at mid and high latitudes. Figure 3(d), representing the PDO modulation of the solar effect, e.g. $(\text{Smax} - \text{Smin})_{\text{PDO}-} - (\text{Smax} - \text{Smin})_{\text{PDO}+}$, shows that the PDO modulates the zonal-mean zonal wind induced by the solar effect over the entire stratosphere, with values significant from the mid-stratosphere down to the upper troposphere. To help understand this PDO modulation, figure 3(d) (green contours) also shows the PDO modulation term in wave forcing. Here the wave forcing is the sum of the planetary wave forcing (the Eliassen–Palm flux

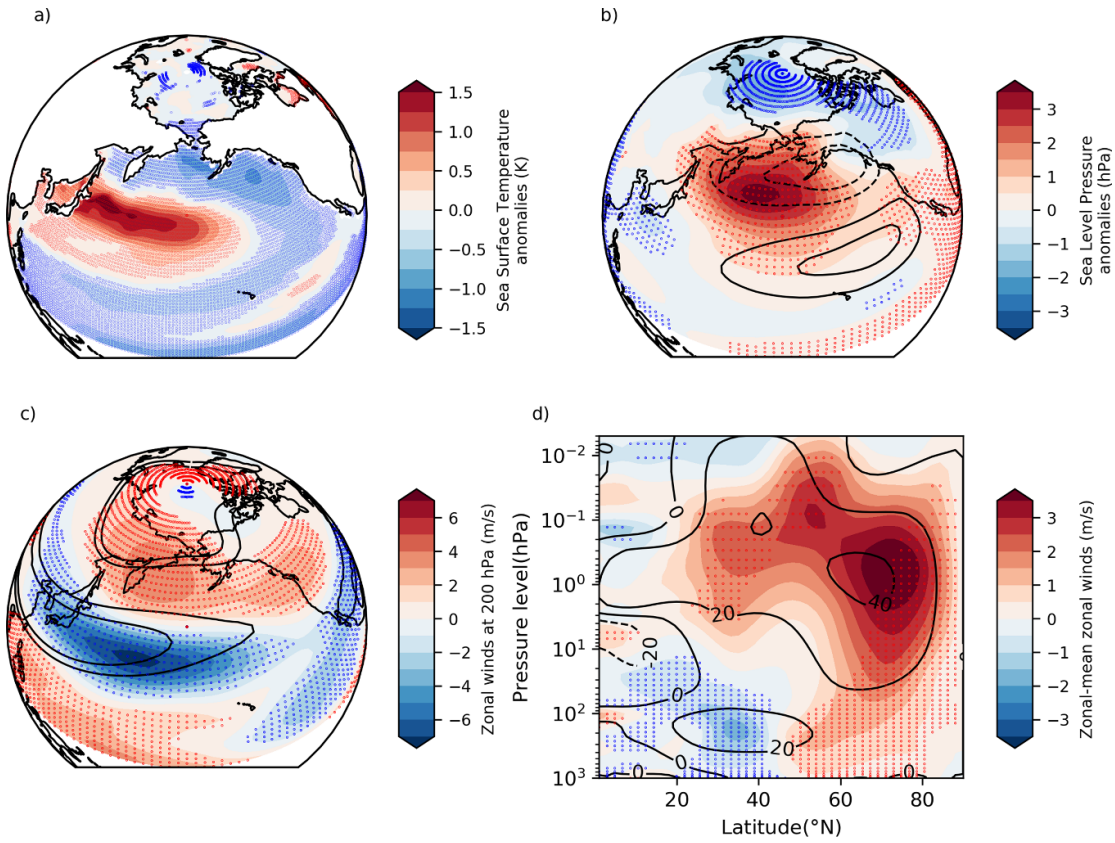

Figure 2. For (PDO− − PDO+) in ND averaged over the ten last years of the simulations, we show in (a) the SST (K), (b) the sea level pressure (SLP, hPa), (c) zonal winds at 200 hPa (m s^{-1}) and (d) zonal-mean zonal winds from surface to the mesopause region (m s^{-1}). Black contours in (b) indicate the climatological SLP anomalies with respect to the zonal mean (−8, −4, 4, 8 hPa) and in (c), (d) the zonal wind climatology (8, 10, 35, 45 m s^{-1} in c). Colored dots indicate the regions where the anomalies are statistically significant (95%).

divergence from waves resolved by the model) and of the parametrized gravity wave drag. The positive wave forcing in the stratosphere indicates an eastward acceleration and corresponds in fact to a decrease of the background planetary wave deceleration (not shown). The negative anomalies aloft in the mesosphere are due to the gravity wave drag, responding opposite to the zonal wind increases below, as commonly found (e.g. Cullens *et al* (2016), Guttu *et al* (2020)). In other words, PDO− preconditions the stratosphere to a state characterized by less planetary wave dissipation and a stronger polar vortex, making the solar response stronger. Figure S3 demonstrates the downward migration of the zonal wind anomalies over the course of the early winter months.

The corresponding differences in the zonal winds at 200 hPa are shown in figures 3(e)–(h). Consistent with figures 3(a)–(d), the solar impact independent of the PDO phase manifests itself as a meridional dipole of anomalies in the subtropical jet exit over the Pacific. Over the Arctic, north of the polar jet, we see a significant strengthening of the zonal winds during the PDO− phase. This is a region where the significant changes are limited to very small areas in during the PDO+ phase or when looking at the PDO independent case. In PDO+, significant wind changes are found in the subtropical jet exit region. The modulation term (figure 3(h)) suggests that the zonal winds are significantly modulated by the PDO phase north of the polar jet, in the Pacific sector of the Arctic. Significant anomalies downstream over North America indicate that the PDO modulation of solar effects in the polar stratosphere may also have notable impacts on tropospheric climate beyond the Pacific sector.

We have now demonstrated that the strength and robustness of the zonal wind changes throughout the stratosphere and troposphere arising from the UV irradiance forcing are strongly dependent on the PDO phase. Figures 4(a)–(d) show the corresponding solar-induced anomalies for SLP. In PDO−, a high SLP anomaly is found straddling the region where the climatological Aleutian Low is located, indicating its weakening. On the contrary, in PDO+, a low SLP anomaly indicates its deepening. These results are broadly consistent with the upper-tropospheric zonal wind anomalies shown in figures 3(f) and (g). There is a cancellation of these two contributions over the Aleutian Low region in the PDO independent component (figure 4(a)).

Earlier model (Ineson *et al* 2011, Gray *et al* 2013, Hood *et al* 2013) and observational (Roy *et al* 2014) studies found a weakened Aleutian Low in Smax.

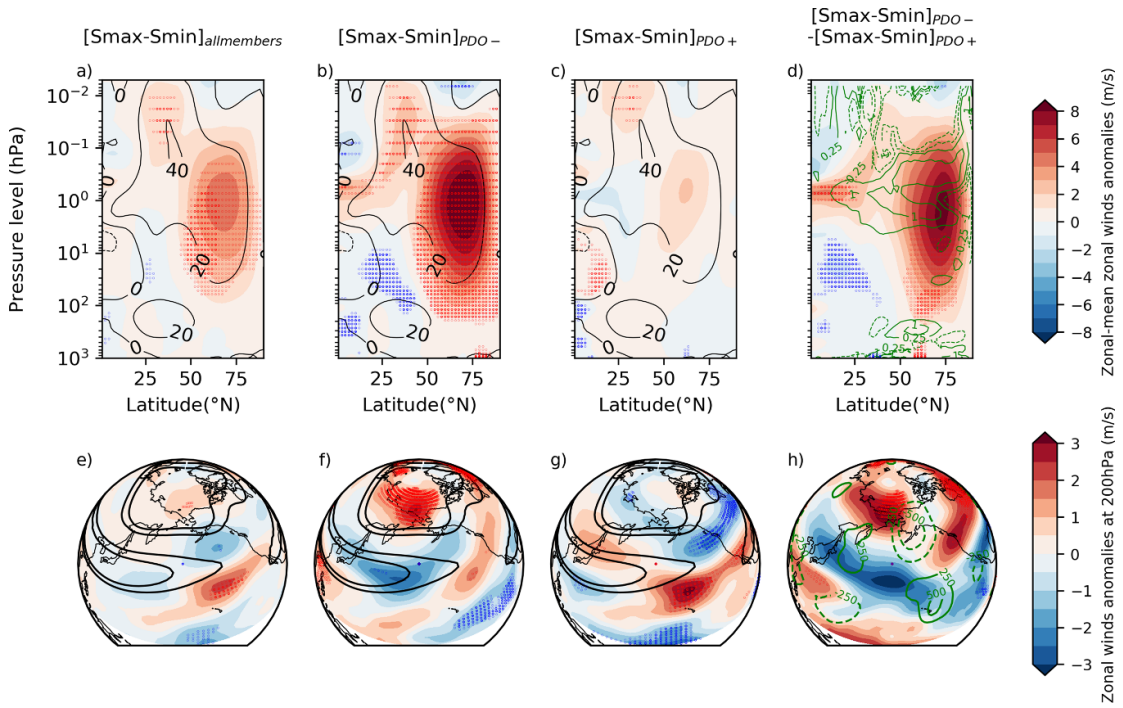

Figure 3. Zonal-mean zonal winds (m s^{-1}) in ND from the surface to the mesopause region and zonal winds at 200 hPa (m s^{-1}) are shown for (a), (e) $(\text{Smax} - \text{Smin})_{\text{allmembers}}$, (b), (f) $(\text{Smax} - \text{Smin})_{\text{PDO}-}$, (c), (g) $(\text{Smax} - \text{Smin})_{\text{PDO}+}$ and (d), (h) $(\text{Smax} - \text{Smin})_{\text{PDO}-} - (\text{Smax} - \text{Smin})_{\text{PDO}+}$ ('modulation term'). In (a)–(c) and (e)–(g), black contours are the zonal wind climatology (8, 10, 35, 45 m s^{-1} in (e)–(g). In (d), (h), green contours indicate the modulation term of the (d) total wave forcing (EP flux divergence + GW drag, m s^{-1} d^{-1}) and (h) the eddy heat flux (m s^{-1}·K). Colored dots (large or small) indicate the regions where the anomalies are statistically significant (95% or 90%).

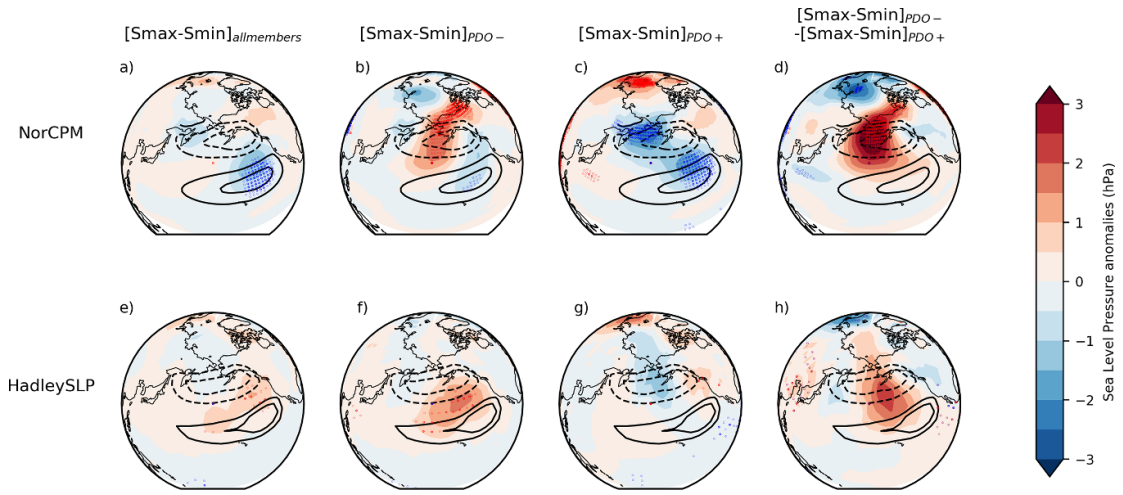

Figure 4. Sea level pressure (SLP, hPa) in ND are shown for the same anomalies as in figure 3, in (a)–(d) for NorCPM and (e)–(h) for Hadley SLP. Black contours indicate the climatological SLP anomalies with respect to the zonal mean (−8, −4, 4, 8 hPa in (a)–(d) and −8, −4, 4, 5.5 in (e)–(g)). Colored dots (large or small) indicate the regions where the anomalies are statistically significant (95% or 90%).

This is supported by the corresponding signatures in the Hadley SLP reanalysis data from 1854 to 2017 (figures 4(e)–(h)). The observational-based results show that the high SLP anomaly corresponding to a weakening of the AL is much more pronounced during PDO−. The SLP solar signature irrespective of the PDO is of the same order of magnitude as found in the aforementioned studies, although it is shown here for ND, while other studies have mostly used DJF-mean (Gray *et al* 2013, Hood *et al* 2013, Roy 2014). There are, however, differences between the model and observations in the exact position of the anomalies. After all, the results over SC 23—under idealized conditions of no other forcings and no QBO—cannot be expected to match the observed mean over 16 solar cycles, derived from the Hadley data. The

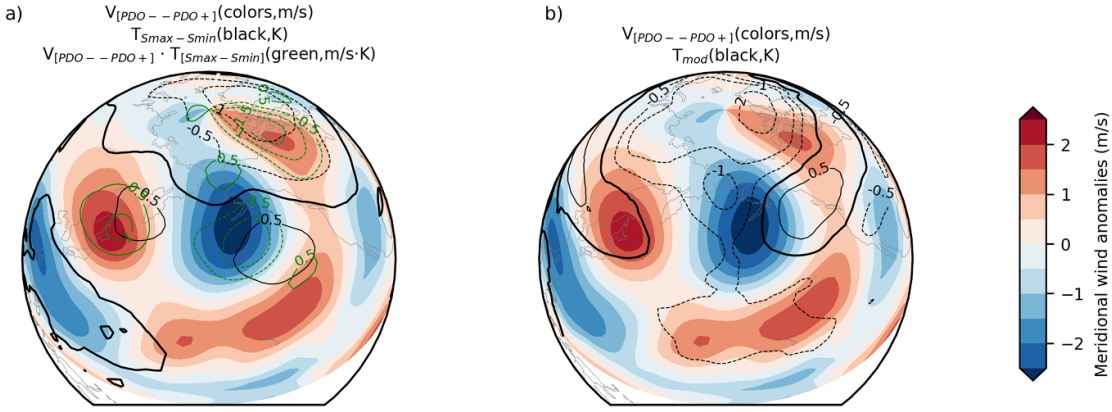

Figure 5. For ND, the meridional winds (shaded contours, m s^{-1}) from (PDO− − PDO+), the temperatures (black contours, K) from (Smax − Smin)$_{allmembers}$ and their product, the meridional heat flux (green contours, m s^{-1}·K), at 200 hPa are shown in (a). The same wind field is shown in (b), while the temperatures (black contours, K) are from (Smax − Smin)$_{PDO-}$ − (Smax − Smin)$_{PDO+}$ ('modulation term').

main point is that there is nevertheless broad agreement on the modulating role of the PDO phase on the North Pacific SLP, as shown in the similarity of the modulation term (figures 4(d) and (h)).

An essential point is now to understand the mechanisms that cause the solar response to amplify during PDO− phases, hence to understand the origin of the modulation term. Figure 5(a) shows the PDO response in meridional winds (shading) along with the solar-induced temperature anomalies (Smax − Smin)$_{allmembers}$, (black contours) both at 200 hPa. The products of these wind and temperature anomalies, the local meridional heat fluxes, are also plotted (green contours). During Smax, colder temperatures are found within the polar cap (figure 5(a)), while weak warm anomalies are found over the North Pacific. The anomalous meridional winds associated with the PDO− (figure 5(a)) advect the solar-induced warm anomalies equatorward (poleward) on the eastern (western) flank of the Aleutian Low. Likewise, poleward advection of cold temperatures occurs over North America. Together, the equatorward advection of warm anomalies and the poleward advection of cold anomalies contribute to predominantly negative (equatorward) heat flux (green contours) over high latitudes of the Pacific and North American region. The zonal mean of this meridional eddy heat flux averaged over high and mid-latitudes is negative (not shown), which implies a reduced vertical component of the EP flux and wave driving of the stratosphere, as supported by figure 3(d). This influence from the PDO, characterized by a reduced meridional heat flux, is consistent with the modulation term for the total eddy heat flux itself (figure 3(h), green contours). Figure 5(b) shows the same meridional wind anomalies as figure 5(a) (shading), but now with the modulation term for temperature at 200 hPa (black contours), i.e. the term that indicates how the PDO modulates the solar temperature response. The negative temperatures over the Arctic surrounded by warm temperatures in the PDO modulation term further demonstrate that the poleward advection of solar-induced cold anomalies over North America and the equatorward advection over the Pacific and their attendant (negative) heat fluxes are important for the reinforcement of the strong polar vortex. In other words, the advection pattern associated with PDO− acts on the solar-induced temperature anomalies to further strengthen the polar vortex through a non-linear feedback.

Until now, we have considered the modulation of the solar response (Smax − Smin) by the PDO. Reciprocally, a pertinent question is to what extent the solar phase is modulating the PDO impact on surface climate. To that end, figure S4 shows the four last terms listed in table 1 for the model SLP, and the corresponding terms for the Hadley data. We reiterate that, by definition, the solar modulation term shown in figure S4(d) is equivalent to the PDO modulation term in figure 4(d). Although the PDO variability induces larger SLP differences than the 11 year solar cycle, the PDO effect in SLP is stronger and encompasses a larger portion of the Aleutian Low in Smax than in Smin (compare figures S4(b), (c), (f), (g)). Overall, figure S4 implies that the solar SSI forcing slightly amplifies the atmospheric and surface impacts from the PDO. The corresponding figure for SSTs (figure S5) demonstrates that the SST anomalies forced by the PDO are far larger and more extensive than those induced by the solar phase, as expected. The similarity of the PDO SST signatures in the two solar phases and the lack of clear large-scale patterns in the modulation term suggest that there is no notable solar influence on the oceanic component of the PDO in our simulations.

4. Summary, discussion and conclusion

In this study, we have investigated to what extent the Pacific climate responds to the UV SSI variability

associated to the 11 year solar cycle and whether this response depends on the PDO phase. We have carried out ensemble simulations comprising 24 members for present-day climate conditions using the high-top chemistry-climate model (WACCM) coupled to an ocean model (MICOM). To isolate the effects from the time-varying UV SSI forcing, we have held forcings from GHGs and volcanic eruptions constant and did not prescribe the QBO. To evaluate the solar effects and their dependency on PDO, we sorted the early winter model output into four categories according to the prevailing solar and the PDO phases. By subtraction and addition of these categories, we have assessed the PDO modulation of solar response upon the stratospheric polar vortex, the Pacific jet stream and the Aleutian Low.

Our results suggest that, in PDO−, the solar impacts are much stronger and more robust than in PDO+. This is reflected by a significantly larger strengthening of the stratospheric polar vortex, stronger positive anomalies in the upper tropospheric zonal winds at high latitudes, north of the polar jet, and a more pronounced weakening of the Aleutian Low. In addition, our results show no clear solar forcing of the PDO oceanic variability of the kind suggested by the apparent synchronization with the observational record (van Loon *et al* 2007).

We infer that Smax and PDO− act in concert to weaken the Aleutian Low and strengthen the stratospheric polar vortex. Hence, the Smax effects are substantially larger in PDO− than in PDO+. In other words, the solar responses depend on the background state set up by the PDO. We found that the climatological conditions in PDO− favor upper tropospheric and lower stratospheric negative meridional heat fluxes, and hence amplify the Arctic cooling, as a result from the interaction between PDO− and Smax. This modulation of wave activity seems to be driven by poleward advection of cold anomalies over northern North America and equatorward advection of warm anomalies over the North Pacific. To our knowledge, this intricate interaction has not been described in previous studies.

The results in Meehl *et al* (2008), (2009) indicated a weakening of the Aleutian Low from the TSI-induced bottom-up effect alone, although they also implied that an adequate representation of top-down effects in the climate models was needed to be quantitatively consistent with observations. Albeit we do not explicitly investigate this tropical TSI pathway in our study, our model simulations (which are performed with a newer version of the atmospheric WACCM model than used in Meehl *et al* (2009), yet with a different ocean model) capture the TSI-related processes which may partly contribute to our total SLP responses over the North Pacific.

Our findings provide new insights in the UV SSI effects on surface climate over the Pacific and globally, with implications for seasonal forecasting and decadal climate prediction. They suggest that the PDO could be a relevant factor to include in multilinear regression studies. Future model studies conducted in a more realistic framework, i.e. including a more comprehensive set of relevant climate forcings, are needed to assess the overall relevance of our results.

Data availability statement

The data that support the findings of this study are available upon reasonable request from the authors.

Acknowledgments

We have been funded by the Norwegian Research Council through Project 255276 (solar effects on natural climate variability in the North Atlantic and Arctic). We acknowledge the UNINETT Sigma2, the National Infrastructure for High-Performance Computing and Data Storage in Norway, for computing resources (NN9206K).

This work was partially supported by the International Space Sciene Institute (ISSI) in Beijing, through the working team "Dynamical signatures of energetic particle precipitation in atmosphere-analyses".

We acknowledge the use of Hadley SLP and NOAA_ERSST_V5 data provided by the NOAA/OAR/ESRL PSL, Boulder, Colorado, USA, from their Web site at https://psl.noaa.gov/.

ORCID iDs

Sigmund Guttu https://orcid.org/0000-0001-8801-1166
Yvan Orsolini https://orcid.org/0000-0001-7454-026X
Frode Stordal https://orcid.org/0000-0002-5190-6473

References

Andrews M B, Knight J R and Gray L J 2015 A simulated lagged response of the North Atlantic Oscillation to the solar cycle over the period 1960–2009 *Environ. Res. Lett.* **10** 054022

Ansell T J *et al* 2006 Daily mean sea level pressure reconstructions for the European-North Atlantic region for the period 1850–2003 *J. Clim.* **19** 2717–42

Ayarzagüena B, Langematz U, Meul S, Oberländer S, Abalichin J and Kubin A 2013 The role of climate change and ozone recovery for the future timing of major stratospheric warmings *Geophys. Res. Lett.* **40** 2460–5

Bentsen M *et al* 2013 The Norwegian Earth System Model, NorESM1-M—part 1: description and basic evaluation of the physical climate *Geosci. Model Dev.* **6** 687–720

Bleck R, Rooth C, Hu D and Smith L T 1992 Salinity-driven thermocline transients in a wind- and thermohaline-forced isopycnic coordinate model of the North Atlantic *J. Phys. Oceanogr.* **22** 1486–505

Coddington O, Lean J L, Pilewskie P, Snow M and Lindholm D 2016 A solar irradiance climate data record *Bull. Am. Meteorol. Soc.* **97** 1265–82

Cullens C Y, England S L and Garcia R 2016 The 11 year solar cycle signature on wave-driven dynamics in WACCM *J. Geophys. Res. Space Phys.* **121** 3484–96
Dong L, Zhou T and Chen X 2014 Changes of Pacific decadal variability in the twentieth century driven by internal variability, greenhouse gases, and aerosols *Geophys. Res. Lett.* **41** 8570–7
Gray L J *et al* 2010 Solar influences on climate *Rev. Geophys.* **48**
Gray L J, Scaife A A, Mitchell D M, Osprey S, Ineson S, Hardiman S, Butchart N, Knight J, Sutton R and Kodera K 2013 A lagged response to the 11 year solar cycle in observed winter Atlantic/European weather patterns *J. Geophys. Res. Atmos.* **118** 13405–20
Guttu S, Orsolini Y, Stordal F, Limpasuvan V and Marsh D R 2020 WACCM simulations: decadal winter-to-spring climate impact on middle atmosphere and troposphere from medium energy electron precipitation *J. Atmos. Sol. Terr. Phys.* **209** 105382
Hood L, Schimanke S, Spangehl T, Bal S and Cubasch U 2013 The surface climate response to 11-yr solar forcing during northern winter: observational analyses and comparisons with GCM simulations *J. Clim.* **26** 7489–506
Hu D and Guan Z 2018 Decadal relationship between the stratospheric Arctic vortex and Pacific decadal oscillation *J. Clim.* **31** 3371–86
Hu D, Guan Z, Tian W and Ren R 2018 Recent strengthening of the stratospheric Arctic vortex response to warming in the central North Pacific *Nat. Commun.* **9**
Huang B, Thorne P W, Banzon V F, Boyer T, Chepurin G, Lawrimore J H, Menne M J, Smith T M, Vose R S and Zhang H M 2017 Extended reconstructed sea surface temperature, version 5 (ERSSTv5): upgrades, validations, and intercomparisons *J. Clim.* **30** 8179–205
Hurwitz M M, Newman P A and Garfinkel C I 2012 On the influence of North Pacific sea surface temperature on the Arctic winter climate *J. Geophys. Res. Atmos.* **117** 1–13
Ineson S, Scaife A A, Knight J R, Manners J C, Dunstone N J, Gray L J and Haigh J D 2011 Solar forcing of winter climate variability in the Northern Hemisphere *Nat. Geosci.* **4** 753–7
Jadin E A, Wei K, Zyulyaeva Y A, Chen W and Wang L 2010 Stratospheric wave activity and the Pacific Decadal Oscillation *J. Atmos. Sol. Terr. Phys.* **72** 1163–70
Kay J E *et al* 2015 The community earth system model (CESM) large ensemble project: a community resource for studying climate change in the presence of internal climate variability *Bull. Am. Meteorol. Soc.* **96** 1333–49
Kodera K and Kuroda Y 2002 Dynamical response to the solar cycle *J. Geophys. Res. Atmos.* **107** 1–12
Kren A C, Marsh D R, Smith A K and Pilewskie P 2016 Wintertime Northern Hemisphere response in the stratosphere to the Pacific decadal oscillation using the Whole Atmosphere Community Climate Model *J. Clim.* **29** 1031–49
Li F, Orsolini Y J, Keenlyside N, Shen M L, Counillon F and Wang Y G 2019 Impact of snow initialization in subseasonal-to-seasonal winter forecasts with the Norwegian Climate Prediction Model *J. Geophys. Res. Atmos.* **124** 10033–48
Li Y, Tian W, Xie F, Wen Z, Zhang J, Hu D and Han Y 2018 The connection between the second leading mode of the winter North Pacific sea surface temperature anomalies and stratospheric sudden warming events *Clim. Dyn.* **51** 581–95
Ma H, Chen H, Gray L, Zhou L, Li X, Wang R and Zhu S 2018 Changing response of the North Atlantic/European winter climate to the 11 year solar cycle *Environ. Res. Lett.* **13** 034007
Mantua N J, Hare S R, Zhang Y, Wallace J M and Francis R C 1997 A Pacific interdecadal climate oscillation with impacts on salmon production *Bull. Am. Meteorol. Soc.* **78**
Marsh D R, Garcia R R, Kinnison D E, Boville B A, Sassi F, Solomon S C and Matthes K 2007 Modeling the whole atmosphere response to solar cycle changes in radiative and geomagnetic forcing *J. Geophys. Res. Atmos.* **112** 1–20
Matthes K *et al* 2017 Solar forcing for CMIP6 (v3.2) *Geosci. Model Dev.* **10** 2247–302
Meehl G A, Arblaster J M and Branstator G 2008 A coupled air–sea response mechanism to solar forcing in the Pacific region *J. Clim.* **21** 2883–97
Meehl G A, Arblaster J M, Matthes K, Sassi F and van Loon H 2009 Amplifying the pacific climate system response to a small 11 year solar cycle forcing *Science* **325** 1114–8
Misios S *et al* 2015 Solar signals in CMIP-5 simulations: effects of atmosphere-ocean coupling *Q. J. R. Meteorol. Soc.* **142** 928–41
Mitchell D M *et al* 2015 Solar signals in CMIP-5 simulations: the stratospheric pathway *Q. J. R. Meteorol. Soc.* **141** 2390–403
Neale R B *et al* 2012 Description of the NCAR community atmosphere model (CAM5) *NCAR Tech. Note* TN-486
Newman M *et al* 2016 The Pacific decadal oscillation, revisited *J. Clim.* **29** 4399–427
Nishii K, Nakamura H and Orsolini Y J 2010 Cooling of the wintertime Arctic stratosphere induced by the western Pacific teleconnection pattern *Geophys. Res. Lett.* **37** 1–6
Orsolini Y J, Karpechko A Y and Nikulin G 2009 Variability of the Northern Hemisphere polar stratospheric cloud potential: the role of North Pacific disturbances *Q. J. R. Meteorol. Soc.* **135** 1020–9
Rind D, Lean J, Lerner J, Lonergan P and Leboissitier A 2008 Exploring the stratospheric/tropospheric response to solar forcing *J. Geophys. Res. Atmos.* **113** 1–25
Roy I 2014 The role of the sun in atmosphere-ocean coupling *Int. J. Climatol.* **34** 655–77
Roy I and Haigh J D 2010 Solar cycle signals in sea level pressure and sea surface temperature *Atmos. Chem. Phys.* **10** 3147–53
Scaife A A, Ineson S, Knight J R, Gray L, Kodera K and Smith D M 2013 A mechanism for lagged North Atlantic climate response to solar variability *Geophys. Res. Lett.* **40** 434–9
Screen J A and Francis J A 2016 Contribution of sea-ice loss to Arctic amplification is regulated by Pacific Ocean decadal variability *Nat. Clim. Change* **6** 856–60
van Loon H, Meehl G A and Shea D J 2007 Coupled air–sea response to solar forcing in the Pacific region during northern winter *J. Geophys. Res. Atmos.* **112** 1–8
Wang Y M, Lean J L and Sheeley N R Jr 2005 Modeling the sun's magnetic field and irradiance since 1713 *Astrophys. J.* **625** 522–38
Wills R C, Schneider T, Wallace J M, Battisti D S and Hartmann D L 2018 Disentangling global warming, multidecadal variability, and El Niño in Pacific temperatures *Geophys. Res. Lett.* **45** 2487–96
Woo S H, Sung M K, Son S W and Kug J S 2015 Connection between weak stratospheric vortex events and the Pacific decadal oscillation *Clim. Dyn.* **45** 3481–92
Yeo K L, Ball W T, Krivova N A, Solanki S K, Unruh Y C and Morrill J 2015 UV solar irradiance in observations and the NRLSSI and SATIRE-S models *J. Geophys. Res. Space Phys.* **120** 6055–70
Yukimoto S, Kodera K and Thiéblemont R 2017 Delayed North Atlantic response to solar forcing of the stratospheric polar vortex *Sci. Online Lett. Atmos.* **13** 53–8